**Supplementary Materials**

**Materials and Methods**

Based on an extensive review of literature sources and news reports, we collected 50 records of sightings or capture of Alligator gars in China, India, Iraq, Philippines, and other countries (Supplementary Table S1). For ecological niche modeling, we collected distribution data of the native Alligator gar population in North America from the Global Biodiversity Information Facility (GBIF, www.gbif.org). We only selected and used data from 2000 to 2020, with a geographical accuracy higher than 1 km. We used Google Earth to eliminate records located on terrestrial land or sea areas as non-representative environmental indicators and used ArcGIS (v10.7) to randomly select samples at a nearest neighbor distance of 5 km (same as the geographical resolution of the environmental variables), resulting in 132 Alligator gar records within its native range. As we suspect this species is in the early stage of invasion in some countries, comprehensive data on its settlement range and time outside its native habitat are limited. Consequently, only records of the native Alligator gar population were used in modeling.

To construct its native ecological niche and assess its potential global invasion risk, we constructed an SDM combining Alligator gar occurrence and various environmental predictors, including climatic, topographic, and hydrological variables. Climatic variables and global elevation were obtained from the WorldClim (v2.1) database. Streamflow data were derived from the Global Streamflow Characteristics Dataset (GSCD_v2.0). Slope features were calculated from elevation in ArcGIS v10.7. Whether a species can persist following establishment depends on species survival probability and reproduction during winter. Furthermore, water temperature is a crucial factor in determining fish distribution. However, as a global water temperature dataset is not currently available, we used temperature-related climatic variables as a reference.

Unlike terrestrial animals, aquatic species are restricted to water bodies. Thus, SDMs are not appropriate if their geographic distribution includes terrestrial areas (Schmidt et al., 2020). Therefore, we set the modeling unit to a grided water body network from a mosaiced global river (Yan et al., 2019) and lake dataset derived from the HydroLAKES dataset (Messager et al., 2016), respectively, resulting in a dataset of 39 variables. All layers were resampled to a spatial resolution of 2.5 min (5 km$^2$) and converted into ASCII format for input into MaxEnt. We used a variance inflation factor (VIF)<16 to remove intercorrelated (Brambilla et al., 2020) and least contributing factors in the model, resulting in 12 variables for construction of the native model (Supplementary Table S2).

We used a maximum entropy-based SDM (MaxEnt v3.4.4) to perform the modeling process (Phillips et al., 2004, 2006). Using a single algorithm, MaxEnt SDMs can accurately predict where an introduced species may establish when projected into a non-native area (Sutton & Martin, 2022). We used 10-fold cross-validation, auto feature function, and ASCII output format, with other settings set to default. We selected models with the lowest corrected Akaike's information criterion (AICc) by setting the model regularization multiplier (RM) from 0.5 to 4 (Brambilla et al., 2020). Area under the receiver operating characteristic (AUC) curve (Fielding & Bell, 1997) and true statistical skill (TSS) were considered as criteria for model validation, where AUC > 0.8 indicates excellent discrimination and TSS < 0 indicates the model is no different from random prediction and +1 indicates perfect performance (Lu et al., 2012).

Finally, we used Jackknife analysis to rank the importance of every environmental variable during the modeling process. As there are few confirmed records of population establishment outside its native range, we built a native model from its original habitat, and projected this to the global scale (Giovanelli et al., 2008). After modeling, the 10th percentile training presence (10PTP) and maximum training sensitivity plus specificity (MTSS) logistic thresholds (Coudrat & Nekaris, 2013) were used to convert the raw outcome into four classes, i.e., no-risk (probability of presence lower than lowest threshold), low-risk (probability of presence between two thresholds), medium-risk (probability of presence higher than highest threshold but lower than 0.8), and high-risk (probability of presence higher than 0.8). We interpreted the highly habitable sustainability range from the optimized model to predict global invasion risk of the Alligator gar.

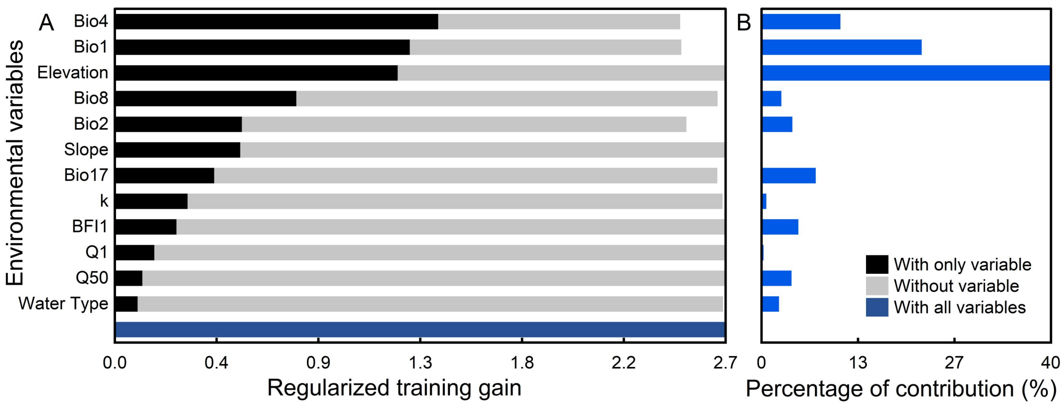


**Supplementary Figure S1 Contribution of environmental variables to native model of Alligator gar**

A: Jackknife analysis of variable-regularized training gain; B: Percentage of each variable's contribution to the model

Supplementary Table S1. Collected invasion reports on Alligator gar

| Latitude | Longitude | Year | Location | Source |
|---|---|---|---|---|
| 37.78935 | 53.90713 | 2008 | Caspian Sea | (Salnikov, 2010) |
| 35.54814 | 46.12197 | 2015 | Marivan Lake, Iran | (Esmaeili, et al., 2017) |
| -6.32785 | 106.64581 | 2016 | Indonesia | GBIF |
| 30.50127 | 47.86588 | 2016 | Basrah, Iraq | (Mutlak, et al., 2017) |
| 22.56906 | 88.39990 | 2016 | West Bengal, Indian | (Manna, et al., 2021) |
| 20.23847 | 85.83521 | 2017 | Odisha, Indian | (Manna, et al., 2021) |
| 18.66399 | 73.48586 | 2018 | Maharashtra, Indian | (Manna, et al., 2021) |
| -8.62833 | 115.10500 | 2019 | Nyanyi Estuary, Indonesia | (Hasan, et al., 2020) |
| -7.30417 | 112.75417 | 2019 | Jagir Sluice, Java Island | (Hasan, et al., 2020) |
| 9.37000 | 76.46000 | 2019 | Kerala, Indian | (Manna, et al., 2021) |
| 16.69671 | 74.27531 | 2019 | Maharashtra, Indian | (Manna, et al., 2021) |
| 23.46358 | 88.34632 | 2020 | Chharaganga Beel, Indian | (Manna, et al., 2021) |
| 26.43037 | 92.01137 | 2020 | Assam, Indian | (Manna, et al., 2021) |
| 17.38408 | 78.37754 | 2021 | Andhra Pradesh, Indian | (Manna, et al., 2021) |
| 1.68030 | 103.90998 | 2022 | Singapore | GBIF |
| 44.50772 | 126.09321 | 2022 | Changchun, Jilin, China | http://news.sohu.com/a/585030288_121123867 |
| 40.05019 | 116.25723 | 2022 | Beijing, China | https://www.163.com/news/article/HFS7LGI60001899N.html |
| 38.88394 | 121.68115 | 2022 | Dalian, Liaoning, China | https://view.inews.qq.com/a/20220928A08UEM00 |
| 38.02121 | 114.66700 | 2022 | Shijiazhuang, Hebei, China | https://www.530311.com/know/show-1281470.html |
| 36.63511 | 101.76440 | 2022 | Xining, Qinghai, China | http://news.hbtv.com.cn/p/2263633.html |
| 28.23312 | 112.93383 | 2022 | Yinchuan, Ningxia, China | https://baijiahao.baidu.com/s?id=1742229989826439701&wfr=spider&for=pc |
| 35.87415 | 120.05229 | 2022 | Qingdao, Shandong, China | https://baijiahao.baidu.com/s?id=1742301629069317241&wfr=spider&for=pc |
| 35.07849 | 118.37214 | 2022 | Linyi, Shandong, China | https://www.baidu.com/link?url=zPZHrH3H7zUsS6YOJTTwxbLHNqkgdE1n4_5Mu-f-aBLKluyrn__Gi1yXRFFtZmLRTuJuHtUR-x6xl7AFMhCNbcBEq4Em1Tq3iiKiu_37ZI3&wd=&eq |

| | | | | |
|---|---|---|---|---|
| | | | | id=fe0d1fcc00036a8e000000036346acc9 |
| 34.16983 | 112.87655 | 2022 | Ruzhou, Henan, China | https://china.cnr.cn/gdgg/20220829/t20220829_525991386.shtml |
| 34.28412 | 117.24551 | 2022 | Xuzhou, Jiangsu, China | https://baijiahao.baidu.com/s?id=1745857721865339544&wfr=spider&for=pc |
| 32.48326 | 119.92266 | 2022 | Taizhou, Jiangsu, China | https://www.163.com/dy/article/HF8HBIF505328YVR.html |
| 32.39194 | 119.37089 | 2022 | Yangzhou, Jiangsu, China | https://baijiahao.baidu.com/s?id=1738653182849687272&wfr=spider&for=pc |
| 32.21164 | 120.58725 | 2022 | Suzhou, Jiangsu, China | https://www.163.com/dy/article/HG16931U0537B1S4.html |
| 33.81105 | 115.77484 | 2022 | Bozhou, Anhui, China | https://www.thepaper.cn/newsDetail_forward_20149354 |
| 33.65831 | 116.96525 | 2022 | Suzhou, Anhui, China | https://m.gmw.cn/baijia/2022-09/18/1303145168.html |
| 31.30574 | 121.47228 | 2022 | Shanghai, China | https://baijiahao.baidu.com/s?id=1743135169123474351&wfr=spider&for=pc |
| 29.83572 | 120.27817 | 2022 | Shaoxing, Zhejiang, China | https://view.inews.qq.com/a/20220830A052M200 |
| 29.45689 | 116.03457 | 2022 | Jiujiang, Jiangxi, China | https://www.sohu.com/a/585519218_162758 |
| 31.03629 | 109.43114 | 2022 | Chongqing, China | https://view.inews.qq.com/k/20220512A00CRX00?web_channel=wap&openApp=false&pgv_ref=baidutw |
| 29.34818 | 104.76957 | 2022 | Nanbu, Sichuan, China | https://baijiahao.baidu.com/s?id=1746367059717950319&wfr=spider&for=pc |
| 28.11542 | 112.76935 | 2022 | Changsha, Hunan, China | https://baijiahao.baidu.com/s?id=1742679291538311810&wfr=spider&for=pc |
| 26.04334 | 119.32077 | 2022 | Fuzhou, Fujian, China | https://www.thepaper.cn/newsDetail_forward_20041938 |
| 24.48946 | 118.10500 | 2022 | Xiamen, Fujian, China | https://c.m.163.com/news/a/H6EOREAJ0512IOAF.html |
| 26.88570 | 100.22441 | 2022 | Lijiang, Yunnan, China | https://share.api.weibo.cn/share/337396342.html?weibo_id=4816577947766758&source=weibolite&wx=1 |
| 25.05009 | 102.70370 | 2022 | Kunming, Yunnan, China | http://news.hbtv.com.cn/p/2263633.html |
| 23.40192 | 110.05921 | 2022 | Guiping, Guangxi, China | https://baijiahao.baidu.com/s?id=1742422900080366502&wfr=spider&for=pc |
| 23.22745 | 113.23967 | 2021 | Guangzhou, Guangdong, China | https://new.qq.com/rain/a/20211105a04fpm00 |
| 23.02341 | 113.78333 | 2021 | Dongguan, Guangdong, China | https://baijiahao.baidu.com/s?id=1718750979177801087&wfr=spider&for=pc |
| 22.59557 | 114.14369 | 2021 | Shenzhen, Guangdong, China | https://www.sznews.com/news/content/2022-08/31/content_25342246.htm |
| 23.11250 | 113.11684 | 2022 | Fuoshan, Guangdong, China | https://baijiahao.baidu.com/s?id=1742765641130820443&wfr=spider&for=pc |
| 23.07116 | 113.05912 | 2022 | Fuoshan, Guangdong, China | https://baijiahao.baidu.com/s?id=1729502609845309146&wfr=spider&for=pc |

| | | | | |
|---|---|---|---|---|
| 22.56889 | 113.89520 | 2022 | Shenzhen, Guangdong, China | https://www.sznews.com/news/content/2022-08/31/content_25342246.htm |
| 19.96390 | 110.31151 | 2022 | Haikou, Hainan, China | https://society.yunnan.cn/system/2022/08/31/032256593.shtml |
| 22.47519 | 114.27210 | 2019 | Hong Kong, China | GBIF |
| 23.97759 | 121.61869 | 2022 | Hualian, Taiwan, China | https://www.baidu.com/link?url=s3pSnBG21A3UlIMEZ1LvokmaxmDKOm49xWsMVZjBEDYfXf381Xoe6RlCXjD6NC6vd2Vi-ahhXa8uo6J0_Sw6E1xJea_JIl19ID_v2ePQStO&wd=&eqid=96cf517600037cde000000036346b0d1 |

Supplementary Table S2. Description and source of environmental variables used in native model building

| Type | Variable | Description | Unit | Source |
|---|---|---|---|---|
| Bioclimatic variables | BIO1 | Annual Mean Temperature | ℃ | WorldClim |
| | BIO2 | Mean Diurnal Range (Mean of monthly (max temp - min temp)) | ℃ | WorldClim |
| | BIO4 | Temperature Seasonality (standard deviation *100) | - | WorldClim |
| | BIO8 | Mean Temperature of Wettest Quarter | ℃ | WorldClim |
| | BIO17 | Precipitation of Driest Quarter | mm | WorldClim |
| Topographic variables | Elevation | | m | Worldclim |
| | Slope | | ° | Calculated from Elevation |
| Hydrological variables | BFI 1 | Baseflow index, defined as the ratio of long-term base flow to total quantitative knowledge of streamflow (Q) | - | GSCD |
| | Q1 | Daily flow that 1% of time in a year exceeded (computed from daily Q data) | mm $day^{-1}$ | GSCD |
| | Q50 | Daily flow that 50% of time in a year exceeded (computed from daily Q data) | mm $day^{-1}$ | GSCD |
| | k | Baseflow recession constant, defined as the rate of baseflow decay | - | GSCD |
| | Water Type | L1: the river that flows into the sea or lake.<br>L2: the river that flows into the L1 river, and its confluence area is larger than one hundredth of the L1 river or 10,000 $km^2$.<br>L3: the river that flows into the L2 river, and its confluence area is larger than one hundredth of the L2 river or 1000 $km^2$.<br>L4: the river that flows into the L3 river, and its confluence area is larger than one hundredth of the L3 river or 100 $km^2$.<br>Lakes are classified into L5 to L7, representing area within 0.1–1, 1–10 and 10–100 $km^2$. | - | (Yan et al., 2019; Messager et al., 2016) |

Supplementary Table S3. The length of river and area of lake from each county that is risky to Alligatior Gar's invasion.

| | | River length (km) | | | Lake area (km$^2$) | | |
|---|---|---|---|---|---|---|---|
| Country name | Country abbreviation | High-risk | Medium-risk | Low-risk | High-risk | Medium-risk | Low-risk |
| China | CHN | 7679.8 | 37466.2 | 5804.9 | 3999.0 | 17413.6 | 861.4 |
| Saudi Arabia | SAU | 8266.9 | 37241.0 | 4230.8 | 0.0 | 7.7 | 0.0 |
| India | IND | 986.2 | 33376.6 | 10632.8 | 378.9 | 3604.0 | 1138.6 |
| Algeria | DZA | 1913.8 | 23785.4 | 14666.1 | 499.8 | 298.3 | 0.0 |
| Pakistan | PAK | 7423.4 | 10093.4 | 1901.3 | 595.4 | 535.7 | 49.7 |
| United States | USA | 89.3 | 10705.6 | 6749.4 | 259.0 | 5674.0 | 2286.1 |
| Mali | MLI | 2682.2 | 10928.9 | 1284.6 | 0.0 | 0.0 | 0.0 |
| Iran | IRN | 620.4 | 7644.4 | 3192.0 | 36.8 | 966.5 | 352.8 |
| Mauritania | MRT | 34.0 | 7341.9 | 2607.9 | 0.0 | 0.0 | 0.0 |
| Iraq | IRQ | 16.0 | 3509.5 | 3267.3 | 282.0 | 5564.1 | 404.7 |
| Australia | AUS | 14.1 | 1624.6 | 5090.0 | 0.0 | 1196.6 | 681.9 |
| Niger | NER | 0.0 | 3452.0 | 3001.9 | 0.0 | 0.0 | 0.0 |
| Vietnam | VNM | 39.8 | 2967.9 | 292.6 | 1.2 | 227.1 | 66.6 |
| Yemen | YEM | 115.2 | 2202.5 | 593.2 | 0.0 | 0.0 | 0.0 |
| United Arab Emirates | ARE | 18.0 | 2540.7 | 30.4 | 0.0 | 39.4 | 0.0 |
| Oman | OMN | 0.0 | 1506.7 | 716.8 | 0.0 | 0.0 | 0.0 |
| Mexico | MEX | 0.0 | 1221.3 | 700.5 | 0.0 | 425.9 | 254.2 |
| Bangladesh | BGD | 0.0 | 158.1 | 987.6 | 0.0 | 244.2 | 44.0 |
| Turkmenistan | TKM | 0.0 | 251.3 | 714.4 | 0.0 | 184.6 | 372.3 |
| Somalia | SOM | 0.0 | 478.7 | 109.0 | 0.0 | 0.0 | 0.0 |
| Ethiopia | ETH | 0.0 | 217.0 | 363.4 | 0.0 | 277.1 | 26.6 |
| Sudan | SDN | 0.0 | 344.2 | 222.6 | 0.0 | 565.7 | 9.0 |
| Nepal | NPL | 0.0 | 431.6 | 114.3 | 0.0 | 0.0 | 0.0 |

| | | | | | | | |
|---|---|---|---|---|---|---|---|
| Egypt | EGY | 0.0 | 391.2 | 79.4 | 0.0 | 3760.0 | 606.3 |
| Djibouti | DJI | 8.9 | 297.1 | 45.6 | 0.2 | 152.0 | 10.9 |
| Afghanistan | AFG | 0.0 | 205.7 | 116.7 | 0.0 | 4.1 | 244.3 |
| Kuwait | KWT | 0.0 | 24.5 | 219.0 | 0.0 | 0.0 | 0.3 |
| Libya | LBY | 0.0 | 61.1 | 161.5 | 0.0 | 0.0 | 0.0 |
| Syrian Arab Republic | SYR | 0.0 | 8.1 | 193.9 | 0.0 | 0.0 | 0.0 |
| Japan | JPN | 0.0 | 59.6 | 125.0 | 0.0 | 1.3 | 66.1 |
| Tunisia | TUN | 0.0 | 27.8 | 123.6 | 0.0 | 0.0 | 0.0 |
| Israel | ISR | 0.0 | 53.3 | 5.7 | 0.0 | 421.8 | 91.8 |
| Jordan | JOR | 0.0 | 33.1 | 15.7 | 0.0 | 432.7 | 81.6 |
| Qatar | QAT | 36.6 | 0.0 | 0.0 | 0.0 | 0.0 | 0.0 |
| Western Sahara | ESH | 0.0 | 0.0 | 7.8 | 0.0 | 0.0 | 0.0 |
| Croatia | CRO | 0.0 | 0.0 | 5.7 | 0.0 | 0.0 | 0.0 |
| Eritrea | ERI | 0.0 | 0.0 | 5.3 | 0.0 | 0.0 | 0.7 |
| Azerbaijan | AZE | 0.0 | 0.0 | 1.5 | 0.0 | 0.0 | 45.9 |
| Morocco | MAR | 0.0 | 0.0 | 1.2 | 0.0 | 0.0 | 0.0 |
| Bahamas | BHS | 0.0 | 0.0 | 0.0 | 0.0 | 0.8 | 14.6 |
| Caspian Sea | - | 0.0 | 0.0 | 0.0 | 0.0 | 311.6 | 730.8 |

Supplementary Table S4. The length of river and area of lake from each province in China that is risky to Alligatior Gar's invasion.

| | River length (km) | | | Lake area ($km^2$) | | |
|---|---|---|---|---|---|---|
| Province | High-risk | Medium-risk | Low-risk | High-risk | Medium-risk | Low-risk |
| Anhui | 545946.6 | 2993237.2 | 1407.8 | 0.0 | 4.1 | 0.3 |
| Fujian | 0.0 | 282264.4 | 54410.0 | 0.0 | 2.3 | 0.6 |
| Guangdong | 68865.0 | 654667.7 | 2215.5 | 0.4 | 4.2 | 0.0 |
| Guangxi | 169147.9 | 234551.2 | 228.5 | 2.5 | 4.3 | 0.1 |
| Guizhou | 0.0 | 1606.9 | 0.0 | 0.0 | 0.6 | 0.6 |
| Hainan | 0.0 | 42332.7 | 42665.0 | 0.0 | 0.3 | 0.1 |
| Henan | 0.0 | 468258.9 | 58742.7 | 0.0 | 1.6 | 1.0 |
| Hubei | 1068886.1 | 1144163.4 | 138173.0 | 0.9 | 2.4 | 0.3 |
| Hunan | 548227.8 | 920339.1 | 24938.8 | 1.9 | 5.7 | 0.3 |
| Jiangsu | 394594.4 | 3603130.0 | 87766.3 | 0.1 | 2.2 | 0.5 |
| Jiangxi | 1199985.8 | 2663666.5 | 2716.4 | 1.9 | 3.1 | 0.0 |
| Shandong | 0.0 | 79501.7 | 318211.2 | 0.0 | 0.0 | 0.1 |
| Shanghai | 0.0 | 53888.4 | 0.0 | 0.0 | 0.2 | 0.0 |
| Sichuan | 0.0 | 49540.7 | 8245.0 | 0.0 | 2.4 | 1.0 |
| Taiwan | 0.0 | 26705.0 | 499.4 | 0.0 | 0.2 | 0.1 |
| Xianggang | 0.0 | 9718.0 | 0.0 | 0.0 | 0.0 | 0.0 |
| Xinjiang | 0.0 | 0.0 | 0.0 | 0.0 | 0.1 | 0.2 |
| Yunnan | 0.0 | 0.0 | 0.0 | 0.0 | 0.1 | 0.1 |
| Zhejiang | 5193.7 | 650222.2 | 75806.8 | 0.0 | 2.1 | 0.3 |
| Chongqing | 0.0 | 818528.4 | 48960.8 | 0.0 | 1.7 | 0.2 |

Supplementary Table S5. The length of river and area of lake from each river basin in China that is risky to Alligatior Gar's invasion.

| | River length (km) | | | Lake area (km$^2$) | | |
|---|---|---|---|---|---|---|
| Province | High-risk | Medium-risk | Low-risk | High-risk | Medium-risk | Low-risk |
| Continental Basin | 0.0 | 0.0 | 0.0 | 0.0 | 0.1 | 0.2 |
| Huaihe River Basin | 0.0 | 4758884.3 | 429426.7 | 0.0 | 6.4 | 1.6 |
| Pearl River Basin | 236009.6 | 1022724.2 | 45068.2 | 2.9 | 9.1 | 0.4 |
| Southeast Basin | 0.0 | 806644.9 | 130717.0 | 0.0 | 4.2 | 1.0 |
| Southwest Basin | 0.0 | 0.0 | 0.0 | 0.0 | 0.005 | 0.006 |
| Yangtze River Basin | 3762834.5 | 10825525.0 | 256172.1 | 4.8 | 17.7 | 2.7 |

**References**


Brambilla M, Scridel D, Bazzi G, Ilahiane L, Iemma A, Pedrini P, et al. 2020. Species interactions and climate change: how the disruption of species co-occurrence will impact on an avian forest guild. *Global Change Biology*, **26**(3): 1212–1224.

Coudrat CN, Nekaris KAI. 2013. Modeling niche differentiation of co-existing, elusive and morphologically similar species: a case study of four macaque species in Nakai-Nam theun national protected area, laos. *Animals* (*Basel*), **3**(1): 45–62.

Esmaeili HR, Masoudi M, Chermahini MA, Esmaeili AH, Zarei F and Ebrahimi M 2017. Invasion of the neotropical and nearctic fishes to Iran. *FishTaxa* **2**(3): 126-133.

Fielding AH, Bell JF. 1997. A review of methods for the assessment of prediction errors in conservation presence/absence models. *Environmental Conservation*, **24**(1): 38–49.

Giovanelli JGR, Haddad CFB, Alexandrino J. 2008. Predicting the potential distribution of the Alien invasive american bullfrog (*lithobates catesbeianus*) in Brazil. *Biological Invasions*, **10**(5): 585–590.

Hasan V, Widodo MS, Islamy RA and Pebriani DA 2020. New records of alligator gar, *Atractosteus spatula* (Actinopterygii: Lepisosteiformes: Lepisosteidae) from Bali and Java, Indonesia. *Acta Ichthyologica et Piscatoria* **50**(2): 233-236.

Lu N, Jia CX, Lloyd H, Sun YH. 2012. Species-specific habitat fragmentation assessment, considering the ecological niche requirements and dispersal capability. *Biological Conservation*, **152**: 102–109.

Manna RK, Ray A, Bayen S, Bera T, Palui D and Das BK 2021. First record of exotic alligator gar, *Atractosteus spatula* (Actinopterygii: Lepisosteiformes: Lepisosteidae), from Ganga river system, India: A possible threat to indigenous riverine fish diversity. *Acta Ichthyologica et Piscatoria* **51**(4): 385–391.

Messager ML, Lehner B, Grill G, Nedeva I, Schmitt O. 2016. Estimating the volume and age of water stored in global lakes using a geo-statistical approach. *Nature Communications*, **7**: 13603.

Mutlak F, Jawad L and Al-Faisal A 2017. *Atractosteus spatula* (Actinopterygii: Lepisosteiformes: Lepisosteidae): A deliberate aquarium trade introduction incidence in the shatt alarab river, Basrah, Iraq. *ACTA Ichthyologica et Piscatoria* **47**(2): 205-207.

Phillips SJ, Anderson RP, Schapire RE. 2006. Maximum entropy modeling of species geographic distributions. *Ecological Modelling*, **190**(3–4): 231–259.

Phillips SJ, Dudík M, Schapire RE. 2004. A maximum entropy approach to species distribution modeling. *In*: Proceedings of the Twenty-First International Conference on Machine Learning. Banff: ACM, 655–662.

Salnikov VB 2010. First finding of gar *Atractosteus* sp. (Actinopterygii, lepisosteiformes, lepisosteidae) in the caspian sea near the coast of turkmenistan. *Russian Journal of Biological Invasions* **1**: 17-20.

Schmidt H, Radinger J, Teschlade D, Stoll S. 2020. The role of spatial units in modeling freshwater fish distributions: comparing a subcatchment and river network approach using MaxEnt. *Ecological Modelling*, **418**: 108937.

Sutton GF, Martin GD. 2022. Testing MaxEnt model performance in a novel geographic region using an intentionally introduced insect. *Ecological Modelling*, **473**: 110139.

Yan DH, Wang K, Qin TL, Weng BS, Wang H, Bi WX, et al. 2019. A data set of global river networks and corresponding water resources zones divisions. *Scientific Data*, **6**(1): 219.